Ms. Ref. No.: EA21-4895R

Cathodic generation of hydrogen peroxide sustained by electrolytic O_2 in a rotating cylinder electrode (RCE) reactor

Oscar M. Cornejo[a,1], Ignasi Sirés[b,1,*], José L. Nava[a,1,**]

[a] *Departamento de Ingeniería Geomática e Hidráulica, Universidad de Guanajuato, Av. Juárez 77, Zona Centro, 36000, Guanajuato, Guanajuato, Mexico*

[b] *Laboratori d'Electroquímica dels Materials i del Medi Ambient, Departament de Química Física, Facultat de Química, Universitat de Barcelona, Martí i Franquès 1-11, 08028 Barcelona, Spai*

* Corresponding author i.sires@ub.edu (I. Sirés)

** Corresponding author: jlnm@ugto.mx (J.L. Nava)

[1] Active ISE Members

Abstract

This investigation reports the electrosynthesis of H_2O_2 from the two-electron reduction of dissolved O_2, provided by anodic water oxidation, in a rotating cylinder electrode (RCE) reactor. O_2 evolved at six surrounding Ti | IrO_2 anode plates, whereas the oxygen reduction reaction (ORR) occurred at a (C-PTFE)-coated carbon cloth covering a rotating steel cathode. The mass transport characterization of the cathodic ORR to yield H_2O_2 was carried out through limiting current measurements (-0.65 ≤ *E* ≤ -0.3 V vs. SHE). Peripheral velocities (*U*) between 11.9 and 79.6 cm s^{-1} (i.e., Reynolds (*Re*) numbers of 4536.5 ≤ *Re* ≤ 30243.1) were employed to ensure turbulent flow conditions. An apparent plateau was obtained in the studied potential range, in agreement with mass transport-controlled ORR. From the limiting current values obtained, the mass transport correlations $k_m a = bU^c$, which describe the transport considering the geometrical aspects of the cell and the hydrodynamic regime, were obtained. Additionally, bulk electrolyses were executed to accumulate H_2O_2, with no O_2 feeding from any air pump. These trials were performed under mass transport control at a cathode potential of -0.46 V vs. SHE. Both, mass transport studies and bulk H_2O_2 electrogeneration, were performed in the presence and absence of atmospheric air on top of the RCE reactor to evaluate the potential contribution of additional O_2 dissolution promoted by the electrolyte velocity and pressure gradients imposed by the RCE. Its contribution to H_2O_2 production depended on *U*. The best conditions for the self-sustained electrolytic H_2O_2 synthesis were *U* = 79.6 cm s^{-1} and cathode potential of -0.46 V, achieving 177.2 mg L^{-1} H_2O_2 with current efficiency and energy consumption of 23.3% and 0.013 kW h (g H_2O_2)$^{-1}$ after 180 min. The potential application of this RCE reactor to the degradation of organic pollutants is thus envisaged.

Keywords: Carbon cloth; Hydrogen peroxide; Mass transport; Oxygen reduction reaction; Rotating cylinder electrode

1. Introduction

Hydrogen peroxide is a widely used chemical for daily domestic and industrial applications [1-3]. The most common route to produce this commodity at an industrial scale is through anthraquinone autoxidation (AO process), which was devised and implemented in the early 1940s [3-5]. For some applications like water treatment via electrochemical advanced oxidation processes (EAOPs), a concentration of H_2O_2 ranging from 3.0 to 15.0 mM is sufficient to attain fast decontamination [2,6-8].

In H_2O_2-EAOPs, the fast degradation of the organic pollutants and their refractory byproducts is feasible because H_2O_2 acts as a clean source of the potent oxidant hydroxyl radical ($^{\bullet}OH$), as H_2O_2 is effectively decomposed by UV light (H_2O_2 photolysis), electron (electrocatalytic reduction), Fe(III)/Fe(II) (electro-Fenton process) or O_3 (electro-peroxone) [9-12]. In these processes, H_2O_2 is produced in situ due to the two-electron oxygen reduction reaction (ORR, reaction (1)) at the cathode surface [6-10].

$$O_2 + 2H^+ + 2e^- \rightarrow H_2O_2 \qquad E^0 = 0.695\ \text{V vs. SHE} \qquad (1)$$

The carbonaceous materials are suitable to carry out the electrosynthesis of H_2O_2, and their selection depends on relevant parameters like the activity and selectivity. In the context of EAOPs, reaction (1) has been mainly carried out using graphite felt (GF), reticulated vitreous carbon (RVC), or carbon cloth (C_{cloth}) coated with C-PTFE [2,5,6,13-18]. Some authors have also developed modified carbonaceous cathodes to enhance the efficiency of reaction (1), as for example, W@Au-decorated and N-doped carbon black [19,20] or (Co,S,P)-decorated and F-doped carbon nanotubes [21,22].

The H_2O_2 electrosynthesis is a critical step in EAOPs since the corresponding H_2O_2 accumulation profiles have significant impact on the performance and stability of the water

treatment. A smart approach to the elucidation of the potential window and the current associated with the ORR (reaction (1)) under mass transport control is based on the experimental obtention of the *I* vs. *E* curves [23]. From these analyses, it is possible to optimize the potential range to carry out the ORR, diminishing the effect of parasitic reactions such as: (i) the cathodic H_2O_2 reduction (reaction (2)); (ii) the four-electron ORR (reaction (3)); and (iii) the hydrogen evolution reaction (HER) (reaction (4)) [15,23-25].

$$H_2O_2 + 2H^+ + 2e^- \rightarrow 2H_2O \qquad E^\circ = 1.801\ \text{V vs. SHE} \tag{2}$$

$$O_2 + 4H^+ + 4e^- \rightarrow 2H_2O \qquad E^\circ = 1.229\ \text{V vs. SHE} \tag{3}$$

$$2H^+ + 2e^- \rightarrow H_2 \qquad E^\circ = 0.0\ \text{V vs. SHE} \tag{4}$$

Furthermore, once the process is controlled by mass transport (i.e., within the plateau of the *I-E* curves), the limiting current (I_L) can be readily identified and related to a volumetric mass transport coefficient ($k_m a$, where the volumetric area is $a = A/V_R$; A is the electrode area, in cm^2, and V_R the electrolyte volume, in cm^3) according to Equation (5):

$$k_m a = \frac{I_L}{2FCV_R} \tag{5}$$

where I_L is in A, 2 is the number of electrons transferred in reaction (1), F is the Faraday constant (= 96,485 C mol^{-1}), and C is the concentration of $O_{2(aq)}$ in bulk (in mol cm^{-3}). As I_L depends on the hydrodynamics within the RCE reactor, the following empirical relationship can be obtained to determine the $k_m a$ dependence on the peripheral velocity (U, in cm s^{-1}) imposed at the RCE:

$$k_m a = bU^c \tag{6}$$

where the constants *b* and *c* are determined from the experimental *I* vs *E* curves. They are associated with the reactor geometry, electrode form, and hydrodynamic flow pattern [23].

In EAOPs, the counter electrode (M) is often an active or non-active anode that promotes the oxygen evolution reaction (OER, the inverse of reaction (3)), with physisorbed or chemisorbed M(•OH) as an intermediate [26,27]. Some anodes, including BDD and certain metal oxides like $BiVO_4$ and $CaSnO_3$, can produce H_2O_2 through water oxidation [28]. However, in most undivided cells like that employed here, active anodes such as Ti|IrO_2 are used because they promote the evolution of O_2 and do not participate very actively in the oxidation of organic compounds [25,28]. Nevertheless, an appropriate design of the electrochemical reactor can turn that shortcoming into an advantage, owing to the H_2O_2 electrosynthesis by reducing the electrolytic (i.e., anodic) O_2 [5,18]. In a recent publication from our research groups, the H_2O_2 accumulation sustained by anodic O_2 evolution was evaluated in a flow-through electrochemical reactor with electrodes configured in a cascade array, achieving an H_2O_2 concentration of 14.3 mg L^{-1} with a current efficiency of 25% and electrolytic energy consumption of 0.021 kW h (g H_2O_2)$^{-1}$ after 180 min of electrolysis [5].

The ability of an RCE to yield H_2O_2 from Equation (1) has been previously explored by the group of Bisang [29,30]. In these works, undivided or divided cells containing a rotating graphite cylinder, which supported three-dimensional electrodes made of either GF or RVC, were employed. An air pump was always used to feed O_2 (at 0.1 MPa) directly to the cathode surface, achieving 8.4 g L^{-1} H_2O_2 with φ = 79% after 6 h using RVC as the cathode in a 0.5 M NaOH solution at 40 mA cm^{-2} and rotation speed (ω) of 1000 rpm [29]. Moreover, the mass transport in RCE reactors has been demonstrated to be outstanding, as demonstrated for metal recovery [31-37]. In this scenario, the electrosynthesis of H_2O_2 through anodically generated O_2 (i.e., with no air pump) is an attractive concept that merits a deeper investigation because, if successful, it would entail a significant cost reduction in practice.

This work describes the electrosynthesis of H_2O_2 at sufficiently high concentration through cathodic ORR from anodically formed O_2 in an RCE reactor. The OER took place at the surface of six active Ti | IrO_2 anodes, whereas the ORR occurred at C_{cloth}, previously hydrophobized with a C-PTFE mixture, fixed on a stainless steel cylinder to ensure the continuity between the materials with high conductivity and a uniform current and potential distribution. The mass transport characterization of the ORR was systematically addressed in the RCE reactor through the measurement of I_L, which was obtained from differential pulse voltammetry (DPV) at U values imposed at the RCE. The influence of peripheral velocity on the H_2O_2 accumulation, current efficiency (φ), electrolytic energy consumption (EC) and normalised space velocity (s_n^{CSTR}) during bulk electrolytic trials at constant cathode potential was also assessed. Furthermore, the mass transport characterization and H_2O_2 electrogeneration studies were carried out both in the presence of atmospheric air (open reactor) or N_2 stream (closed reactor) on top, aiming to fully describe the contributions to H_2O_2 production.

2. Experimental

The reagents employed in this work were of analytical grade. They were acquired from Sigma-Aldrich and Karal and used as received. All the solutions to carry out the analyses and electrolytic trials were prepared with distilled water.

2.1 Description of the reactor

Fig. 1a shows the electrochemical reactor containing an RCE cathode, made of a 316-type stainless steel cylinder covered with a C_{cloth} (Sainergy^{TM}) coated with C-PTFE (ohmic resistance of 1.1 Ω between the materials), and six Ti | IrO_2 plates as the anodes. The stainless

steel cylinder had a diameter (*d*) of 3.8 cm, a wall thickness of 1 mm and a length of 11 cm (Fig. 1b), and the geometric area exposed to the electrolyte of the adapted C_{cloth} was 120 cm^2. On the other hand, each Ti | IrO_2 plate anode had 13 cm length × 2 cm width × 0.3 cm thickness. The set of pieces provided 120 cm^2 of total geometric area in contact with the electrolyte. The six Ti | IrO_2 plates were attached to the internal wall of the reactor using a polymer ring, which acted as a holder at the top of the glass vessel, and they were fastened with screws. The Ti | IrO_2 anodes were fabricated via the Pechini method as previously described by ourselves [38]. The glass vessel (internal diameter of 8.3 cm and 11.0 cm in depth) contained 500 cm^3 of solution volume in each trial. The RCE reactor was operated in batch mode. An electric motor with variable rotation speed and a power of 0.11 hp (IKA, model RW 20) was employed to rotate the coated C_{cloth} RCE. A saturated mercury/mercurous sulfate reference electrode was placed in the interelectrode gap to control the applied cathode potential. All the potentials mentioned in this work are referred to the standard hydrogen electrode (SHE).

2.2 Instruments and analytical procedures

All the electrochemical trials were carried out using an SP 150 potentiostat-galvanostat coupled to an external booster VMP3B-10 from BioLogic®. The EC-Lab® software was employed to obtain the data from the electrolyses. The dissolved oxygen concentration was measured with a Hanna® HI 9142 dissolved oxygen meter. The accumulated H_2O_2 concentration was quantified by the Ti(IV)-H_2O_2 complex colorimetric method, using a Perkin-Elmer Lambda 35 UV/Vis spectrophotometer set at λ = 408 nm [39].

2.3 Mass transport characterization for the ORR through DPV analysis

The reactor with working, counter and reference electrodes described in subsection 2.1 was employed. DPV measurements at different peripheral velocities imposed at the C_{cloth} RCE were performed to identify the potential range at which the I_L plateau associated with the ORR (reaction (1)) appeared. The peripheral velocities were imposed via the rotational frequency f ($U = 2\pi fr/60$, where f is expressed in rev min^{-1}, r is the RCE radius in cm and 60 is a conversion factor to yield U in cm s^{-1}). In this voltammetric study, a 0.5 M Na_2SO_4 solution at pH 3 was employed. Prior to the electrochemical measurements, the solution was aerated until the maximum solubility of O_2 (0.25 mM at 298 K) was reached. This took about 20 min and then, in most of the assays an air blanket was maintained over the liquid to ensure a constant dissolved O_2 concentration. Note that the DPV technique allows diminishing the effect of the capacitive current, which is relevant at diluted concentrations ($< 10^{-4}$ M), resulting in clearer voltammetric signals that simplify the identification of the expected plateau.

The working electrode (i.e., cathode) potential was swept from the open circuit value (0.31 V vs. SHE) to -1.8 V vs. SHE. The scan rate was fixed at 5 mV s^{-1}, with a pulse height of 1.0 mV and a pulse width 5.0 ms. Two different sets of trials were performed: (i) With the RCE reactor open to the air stream in order to allow the O_2 dissolution (thus emulating the natural influx of O_2 occurring in bulk electrolyses, see below), or (ii) using an N_2 stream on top of the reactor (i.e., closed reactor) to impede the additional O_2 access and dissolution.

2.4 Bulk electrolysis

The H_2O_2 accumulation tests were carried out using 500 cm^3 of a 0.05 M Na_2SO_4 solution at pH 3 and 298 ± 2 K. The effect of both U (11.9–79.6 cm s^{-1}) in the open reactor and N_2 overlying atmosphere (closed reactor) was evaluated. The electrolyses were carried

out under potentiostatic conditions applying a cathode potential (E_{cath}) of -0.46 V vs. SHE at the C_{cloth} RCE. This value was chosen from the plateau identified in trials described in the previous subsection. Note that the electrolyses were performed under turbulent flow regime, at Reynolds number ($Re = dU/\nu$) comprised within the range of $4537 \leq Re \leq 30243$, being d and ν the RCE diameter and electrolyte kinematic viscosity (= 0.001 $cm^2\ s^{-1}$).

From the H_2O_2 accumulation tests made at a constant potential, the φ and the EC were calculated as follows:

$$\varphi = \frac{2F\Delta C_{H_2O_2}V}{1000M_{H_2O_2}It} \times 100 \quad (7)$$

$$\mathrm{EC} = \frac{E_{cell}It}{3600\Delta C_{H_2O_2}V} \quad (8)$$

where 2 is the number of electrons transferred in Equation (1), $C_{H_2O_2}$ is the accumulated hydrogen peroxide concentration (in mg L^{-1}), V is the solution volume (in L), 1000 is a factor in homogenizing units, $M_{H_2O_2}$ is the molecular weight of H_2O_2 (34.01 g mol^{-1}), I is the applied current (in A) obtained from the bulk electrolysis chronoamperograms, t is the electrolysis time (in s), and 100 is a conversion factor for obtaining the efficiency as a percentage. In Eq. (8), E_{cell} is the cell voltage (in V), and 3600 is a conversion factor to attain units of kW h $(g\ H_2O_2)^{-1}$.

3. Results and discussion

3.1 Mass transport characterization via measurements of limiting current during the ORR

The RCE reactors are suitable for performing several studies, such as the electrosynthesis of chemicals in a turbulent flow regime. Turbulence in these reactors is reached at *Re* as low as 100, in contrast to other cell configurations, which typically reach turbulent regime at

higher values (e.g., $Re > 10^6$ and $Re > 2300$ using rotating disc and parallel plate electrodes, respectively). Turbulence improves mass transport, which is beneficial for the electrolysis of dilute solutions, as is the case of this research (see subsection 2.4).

Fig. 2a shows the DPV curves obtained for the cathodic reduction of dissolved O_2 at the RCE in the presence of air on top of the RCE reactor (open reactor) at different U values. The appearance of a plateau, attributed to the ORR under mass transport control, can be observed globally within the potential range $-0.65 < E_{cath} < -0.3$ V in all the assays. However, these limits were dependent on the U value, as the plateau started at -0.3 V at 11.9 cm s^{-1} but its origin was gradually shifted to more negative values, starting at -0.46 V when U was 79.6 cm s^{-1}. This can be explained by the enhanced O_2 influx to the RCE at higher U, which takes a longer time to become stable. It is also important to mention that at $E < -0.7$ V, a considerable current increase was identified regardless of U, which can be accounted for by the start of the parasitic HER (reaction (4)), and H_2O_2 reduction reaction (2). The obtention of the optimum E_{cath} interval is thus crucial to enhance the selectivity of reaction (1). The second key effect of the increased rotation speed was that progressively greater I_L values were obtained, rising from 167 to 259 mA at $E_{cath} = -0.46$ V (chosen because in all trials, this potential was in the plateau zone) when U was increased from 11.9 to 79.6 cm s^{-1}, respectively. This means that the activity of the RCE made of C_{cloth} rises as the O_2 feeding is promoted by the greater rotation within the studied U range. It can then be concluded that both, the selectivity and the activity for the two-electron ORR, were substantially enhanced as U was risen, thereby expecting a higher Faradaic efficiency for H_2O_2 production in bulk electrolyses (see below).

The RCE rotation, especially at high speed, could presumably induce a surplus dissolution of O_2 associated with the suction effect that pulls atmospheric air into the solution.

Fig. 2b shows the *I* vs. *E* curves recorded under analogous conditions of those of Fig. 2a but using an N_2 overlying atmosphere (closed reactor). As can be seen, the same plateau attributed to the mass transport-controlled ORR is observed, showing a similar potential window when comparing with Fig. 2a at each corresponding *U* value. Nonetheless, the I_L obtained using the inert top atmosphere was clearly diminished at the lowest peripheral velocities. For example, it attained 142 mA instead of 167 mA at E_{cath} = -0.46 V and 11.0 cm s^{-1} (Fig. 2b), which corroborates the role of overlying air as a source of dissolved O_2. Such decrease was not observed at the highest *U* values, as verified at 79.6 cm s^{-1} (262 mA instead of 259 mA), which can be accounted for by the comparatively greater influx of anodic O_2 that makes the atmospheric O_2 contribution irrelevant. This means that even if suction is smaller at low *U*, its influence is more significant.

Aiming at completing this voltammetric study, DPV curves were also recorded using the same stainless steel RCE but in the absence of the C_{cloth} (not shown herein). The ORR plateau did not appear, which means that O_2 was reduced to water. The (C-PTFE)-coated C_{cloth} is thus the active material needed to produce H_2O_2 (reaction (1)).

The volumetric mass transport coefficients were determined using the I_L values obtained from experiments shown in Fig. 2a and 2b, at each peripheral velocity, according to Eq. (5). Fig. 3 shows the logarithmic $k_m a$ vs. *U* plot for the trials performed with the open and close RCE reactor. It can be noticed that, in the range of $11.9 \leq U \leq 59.7$ cm s^{-1}, the $k_m a$ values were higher when the reactor was open to the atmosphere, in agreement with the discussion made from Fig. 2 that confirmed the positive contribution of atmospheric O_2 to the ORR. However, the superior O_2 conversion to H_2O_2 was gradually less evident as *U* rose and, in fact, at 70.0 and 79.5 cm s^{-1}, the $k_m a$ values became similar in the presence and absence of

atmospheric air. This confirms the aforementioned finding that at higher *U*, the transport of the dissolved anodic O_2 is much faster than the air suction phenomenon caused by the RCE rotation. Table 1 summarizes the mass transport correlations ($k_m a = bU^c$) for the (C-PTFE)-C_{cloth}-covered RCE, showing the values of the *b* and *c* constants calculated through the analysis of the experimental data of Fig. 3. The value of constant *b* is higher for trials made in the presence of atmospheric air, in agreement with the positive contribution of the atmospheric O_2 to the overall O_2 mass transport that determines the ORR. On the other hand, the values of the superscript *c* were 0.22 and 0.31 for the trials in the open and closed RCE reactor, respectively. Note that these values are lower than expected for electrolyses performed in the RCE reactor under turbulent flow regime, where *c* is typically greater than 0.7 [31-33]. Such a substantial decrease can be attributed to the dilute concentration of dissolved O_2 (0.25 mM), whereas solutions employed for metal recovery in this reactor usually contain metal ions with a concentration in the molar range.

The mass transport correlations obtained in this study are analogous to those found in a previous communication focused on the ORR from dissolved O_2 using 2D and 3D carbonaceous cathodes fitted in a filter-press cell and shown in Table 1 [23]. However, the mass transport was some order of magnitude greater when three-dimensional electrodes like RVC and GF were employed, owing to the high volumetric area provided by these materials [23].

3.2 H_2O_2 accumulation in the RCE reactor using anodically generated O_2

In this set of experiments, unlike those shown in the previous mass transport characterization studies, the electrolytic oxygen generated at the Ti$|$$IrO_2$ anodes was the main oxygen source to produce H_2O_2. The electrolyses were performed using the open RCE

reactor, which allowed the dissolution of atmospheric O_2. Hence, a preliminary saturation of the solution with an airstream was not needed. The influence of peripheral velocity on the accumulation of dissolved O_2 and H_2O_2 was investigated at a constant E_{cath} = -0.46 V vs. SHE applied to the (C-PTFE)-C_{cloth} RCE, as this potential ensured that the ORR was always controlled by mass transport (Fig. 1). The trials were carried out using a solution containing 0.05 M Na_2SO_4 at pH 3 at 298 ± 2 K, which is a medium widely used to compare the performance of different materials and reactors related to H_2O_2 electrogeneration and H_2O_2-based EAOPs [6,17,22,25].

First, the influence of the peripheral velocity on the dissolved O_2 concentration, which was partly generated at the Ti | IrO_2 anodes, was analyzed during the electrosynthesis of H_2O_2. The dissolved O_2 was measured at t = 15 min, once a steady value was reached. Fig. 4 shows the O_2 concentration decay as the peripheral velocity was increased, yielding values from 13.5 mg L^{-1} O_2 (0.42 mM) to 8 mg L^{-1} O_2 (0.25 mM) in the interval of U from 11.9 to 59.7 cm s^{-1}. The depletion of dissolved O_2 in the electrolyte at higher U can be explained by its faster mass transport towards the cathode, facilitating its reduction to H_2O_2. It is evident, however, that the turbulence generated by increasing the peripheral velocity favors the O_2 dissolution, promoting its supersaturation in the electrolyte (O_2 solubility from air is ~8 mg L^{-1}), which guarantees the continuous accumulation of H_2O_2 as further investigated.

Fig. 5a shows the H_2O_2 concentration (in mg L^{-1} and in mM) accumulated for 180 min. It is evident that the ORR (reaction (1)) can be sustained autonomously thanks to the transport of the anodic O_2. Furthermore, it can be observed that the H_2O_2 accumulation increased as a function of the peripheral velocity, owing to the faster transport of the $O_{2(aq)}$ towards the RCE. This is in full agreement with the mass transport characterization, as higher I_L values

resulted at greater *U* (Fig. 3). The final H_2O_2 concentration changed from 19.8 to 177.2 mg L^{-1} (> 5 mM) when *U* rose from 11.9 to 79.6 cm s^{-1}. The sharp enhancement found when *U* was increased from 19.9 to 39.8 cm s^{-1} (Fig. 5a) informs about the essential role played by the hydrodynamics in the ORR, as this reaction is totally dependent on the efficient transport of anodic O_2 towards the cathode. If the rotation speed is too low ($U \leq 19.9$ cm s^{-1}), a small fraction of anodic O_2 arrives at the cathode surface since the rest moves to the gas phase. As depicted in Fig 5b, the current efficiency also became greater at higher *U* values, which agrees with the enhanced selectivity and activity discussed in Fig. 2. In most cases, the efficiency was greater at the beginning of the trials, whereupon it progressively decayed. This is particularly evident at the highest *U* values, and it is explained by the simultaneous partial anodic destruction of the accumulated H_2O_2 (i.e., the inverse of reaction (1)). The φ values at 180 min for this set of experiments were 5.2%, 5.9%, 21.7%, 22.1%, and 23.3%. Conversely, the energy consumption (just considering the energy needed to run the electrolysis) became lower at higher *U*. Thus, the EC values were 0.060, 0.050, 0.015, 0.014 and 0.013 kW h $(g\ H_2O_2)^{-1}$ at *U* rising from 11.9 to 79.6 cm s^{-1} (Fig. 5c). Note that the modest final current efficiencies are attributed to the concomitant anodic H_2O_2 destruction alongside the cathodic parasitic reactions (2)-(4). For completeness sake, the normalised space velocity was calculated from the following expression [40]:

$$s_{\mathrm{n}}^{\mathrm{CSTR}} = \frac{k_{\mathrm{m}} a}{0.9} \tag{9}$$

This parameter allows determining the electrolyte volume in which the reactant conversion reaches 90% per unit volume of the reactor and per unit time [40]. The RCE was treated as a continuously stirred tank reactor (CSTR) in batch operation mode. The obtained

s_n^{CSTR} values were 7.69 × 10^{-3}, 9.21 × 10^{-3}, 1.05 × 10^{-2}, 1.13 × 10^{-2} and 1.19 × 10^{-2} m^3 m^{-3} s^{-1} at *U* of 11.9, 19.9, 39.8, 59.7, and 79.6 cm s^{-1}, respectively.

The second set of experiments was performed to corroborate or discard the positive influence of the atmospheric O_2 found and discussed during the mass transport characterization. These assays were made in the closed RCE reactor, under the same experimental conditions of tests in Fig. 5a but maintaining a controlled N_2 atmosphere above the liquid surface to prevent the dissolution of atmospheric O_2. Fig. 6a highlights that the overall accumulation of H_2O_2 was lower in this reactor as compared to the open reactor (Fig. 5a), confirming that the peripheral velocity promotes the suction of O_2 from the atmosphere, enhancing the dissolved O_2 concentration and eventually facilitating the two-electron ORR. The H_2O_2 concentration accumulated at 180 min changed from 17.0 to 160.5 mg L^{-1} (< 5 mM) when *U* rose from 11.9 to 79.6 cm s^{-1}. It is worth mentioning that the relative influence of the additional O_2 dissolution on the H_2O_2 accumulation was greater at lower *U* values, which is coherent with conclusions drawn from Fig. 2. For example, at 11.9 and 19.9 cm s^{-1}, the difference in final H_2O_2 concentrations between trials with and without overlying O_2 was 14% and 19%, whereas at 39.8-79.6 cm s^{-1} the difference was below 10%.

From the poorer electrogeneration ability in the presence of N_2, it can be easily inferred that lower φ (4.8%-21.1%) and higher EC (0.065-0.015 kW h (g H_2O_2)$^{-1}$) values were determined at 180 min (Fig. 6b and 6c). The s_n^{CSTR} values were 6.54 × 10^{-3}, 8.02 × 10^{-3}, 9.03 × 10^{-3}, 1.06 × 10^{-2}, and 1.22 × 10^{-2} m^3 m^{-3} s^{-1} at *U* increasing from 11.9 to 79.6 cm s^{-1}. The values at *U* < 79.6 cm s^{-1} are clearly lower than those determined with the RCE reactor open to the atmosphere (see above), owing to the significantly poorer mass transport (Fig. 3), whereas the s_n^{CSTR} became almost equal at the highest *U* tested.

The feasibility of H_2O_2 production in an RCE reactor without requiring an air pump as the O_2 source has been demonstrated. Even though the current efficiency was between 5% and 23 % at the end of the electrolysis, the results presented in this work constitute the first step toward their implementation in water treatment by EAOPs, such as electro-Fenton and electro-peroxone processes that are currently under investigation. It is expected that the RCE reactor will provide good performance in EAOPs, where the H_2O_2 is continuously consumed during the water treatment, avoiding its decomposition on the electrodes. In this context, treatments in continuous mode would also minimize the H_2O_2 destruction at the electrodes.

4. Conclusions

The mass transport characterization of dissolved O_2 referred to the promotion of the two-electron ORR was made from cathodic polarization curves, which revealed that E_{cath} = -0.46 V was optimum to operate under mass transport control. Moreover, the positive effect of atmospheric air on mass transport was confirmed from the corresponding correlations. This analysis showed that a greater peripheral velocity (rotation speed) at the (C-PTFE)-C_{cloth} RCE favors the mass transport of dissolved O_2 toward the cathode surface, enhancing the H_2O_2 synthesis. Additionally, the bulk electrolyses carried out to produce H_2O_2, sustained by the O_2 formed at the Ti | IrO_2 anodes, demonstrated the large ability of the system to accumulate a sufficiently high concentration: over 5 mM H_2O_2 at 79.6 cm s^{-1} after 180 min, with current efficiency and energy consumption of 23.3% and 0.013 kW h (g H_2O_2)$^{-1}$, respectively. The results suggest that the RCE reactor could be used in H_2O_2-based water treatment to eliminate persistent organic pollutants via hydroxyl radicals.

Acknowledgments

The authors are glad to thank the financial support from the University of Guanajuato (Mexico) through project CIIC 167/2021, as well as from PID2019-109291RB-I00 (MCIN/AEI/ 10.13039/501100011033, Spain) project.

References

[1] K. Dong, Y. Lei, H. Zhao, J. Liang, P. Ding, Q. Liu, Z. Xu, S. Lu, Q. Li, X. Sun, Noble-metal-free electrocatalysts toward H_2O_2 production, J. Mater. Chem. A 8 (2020) 23123-23141.

[2] Q. Zhang, M. Zhou, G. Ren, Y. Li, Y. Li, X. Du, Highly efficient electrosynthesis of hydrogen peroxide on a superhydrophobic three-phase interface by natural air diffusion, Nature Commun. 11 (2020) 1731.

[3] W. Zhou, L. Xie, J. Gao, R. Nazari, H. Zhao, X. Meng, F. Sun, G. Zaho, J. Ma, Selective H_2O_2 electrosynthesis by O-doped and transition-metal-O-doped carbon cathodes via O_2 electroreduction: A critical review, Chem. Eng. J. 410 (2021) 128368.

[4] S. Yang, A. Verdaguer-Casadevall, L. Arnarson, L. Silvioli, V. Čolić, R. Frydendal, J. Rossmeisl, I. Chorkendorff, I.E.L. Stephens, Toward the decentralized electrochemical production of H_2O_2: A focus on the catalysis, ACS Catal. 8 (2018) 4064-4081.

[5] O.M. Cornejo, I. Sirés, J.L. Nava, Electrosynthesis of hydrogen peroxide sustained by anodic oxygen evolution in a flow-through reactor, J. Electroanal. Chem. 873 (2020) 114419.

[6] G. Daniel, Y. Zhang, S. Lanzalaco, F. Brombin, T. Kosmala, G. Granozzi, A. Wang, E. Brillas, I. Sirés, C. Durante, Chitosan-derived nitrogen-doped carbon electrocatalyst for

a sustainable upgrade of oxygen reduction to hydrogen peroxide in UV-assisted electro-Fenton water treatment, ACS Sustain. Chem. Eng. 8 (2020) 14425-14440.

[7] J. Wang, C. Li, M. Rauf, H. Luo, X. Sun, Y. Jiang, Gas diffusion electrodes for H_2O_2 production and their applications for electrochemical degradation of organic pollutants in water: A review, Sci. Total Environ. 759 (2021) 143459.

[8] W. Zhou, X. Meng, J. Gao, A.N. Alshawabkeh, Hydrogen peroxide generation from O_2 electroreduction for environmental remediation: A state-of-the-art review, Chemosphere 225 (2019) 588-607.

[9] O.M. Cornejo, J.L. Nava, Mineralization of the antibiotic levofloxacin by the electro-peroxone process using a filter-press flow cell with a 3D air-diffusion electrode, Sep. Purif. Technol. 254 (2021) 117661.

[10] A.A. Márquez, I. Sirés, E. Brillas, J.L. Nava, Mineralization of Methyl Orange azo dye by processes based on H_2O_2 electrogeneration at a 3D-like air-diffusion cathode, Chemosphere 259 (2020) 127466.

[11] W. Yang, M. Zhou, L. Mai, H. Ou, N. Oturan, M.A. Oturan, E.Y. Zeng, Generation of hydroxyl radicals by metal-free bifunctional electrocatalysts for enhanced organics removal, Sci. Total Environ. 791 (2021) 148107.

[12] Q. Yang, H. Huang, K. Li, Y. Wang, J. Wang, X. Zhang, Ibuprofen removal from drinking water by electro-peroxone in carbon cloth filter, Chem. Eng. J. 415 (2021) 127618.

[13] P.A. Diaw, N. Oturan, M.D. Gaye Seye, O.M.A. Mbaye, M. Mbaye, A. Coly, J.-J. Aaron, M.A. Oturan, Removal of the herbicide monolinuron from waters by the electro-Fenton treatment, J. Electroanal. Chem. 864 (2020) 114087.

[14] S. Lanzalaco, I. Sirés, M.A. Sabatino, C. Dispenza, O. Scialdone, A. Galia, Synthesis of polymer nanogels by electro-Fenton process: investigation of the effect of main operation parameters, Electrochim. Acta 246 (2017) 812-822.

[15] T. Pérez, G. Coria, I. Sirés, J.L. Nava, A.R. Uribe, Electrosynthesis of hydrogen peroxide in a filter-press flow cell using graphite felt as air-diffusion cathode, J. Electroanal. Chem. 812 (2018) 54-58.

[16] I. Salmerón, K.V. Plakas, I. Sirés, I. Oller, M.I. Maldonado, A.J. Karabelas, S. Mato, Optimization of electrocatalytic H_2O_2 production at pilot plant scale for solar-assisted water treatment, App. Catal. B: Environ. 242 (2019) 327-336.

[17] A. Thiam, R. Salazar, E. Brillas, I. Sirés, In-situ dosage of Fe^{2+} catalyst using natural pyrite for thiamphenicol mineralization by photoelectro-Fenton process, J. Environ. Manage. 270 (2020) 110835.

[18] W. Zhou, L. Rajic, Y. Zhao, J. Gao, Y. Qin, A.N. Alshawabkeh, Rates of H_2O_2 electrogeneration by reduction of anodic O_2 at RVC foam cathodes in batch and flow-through cells, Electrochim. Acta 277 (2018) 185-196.

[19] V.S. Antonin, L.S. Parreira, L.R. Aveiro, F.L. Silva, R.B. Valim, P. Hammer, M.R.V. Lanza, M.C. Santos, W@Au nanostructures modifying carbon as materials for hydrogen peroxide electrogeneration, Electrochim. Acta 231 (2017) 713-720.

[20] J. Lu, X. Liu, Q. Chen, J. Zhou, Coupling effect of nitrogen-doped carbon black and carbon nanotube in assembly gas diffusion electrode for H_2O_2 electro-generation and recalcitrant pollutant degradation, Sep. Purif. Technol. 265 (2021) 118493.

[21] W. Wang, X. Lu, P. Su, Y. Li, J. Cai, Q. Zhang, M. Zhou, O. Arotiba, Enhancement of hydrogen peroxide production by electrochemical reduction of oxygen on carbon nanotubes modified with fluorine, Chemosphere 259 (2020) 127423.

[22] Z. Ye, D.R.V. Guelfi, G. Álvarez, F. Alcaide, E. Brillas, I. Sirés, Enhanced electrocatalytic production of H_2O_2 at Co-based air-diffusion cathodes for the photoelectro-Fenton treatment of bronopol, Appl. Catal. B: Environ. 247 (2019) 191-199.

[23] G. Coria, T. Pérez, I. Sirés, J.L. Nava, Mass transport studies during dissolved oxygen reduction to hydrogen peroxide in a filter-press electrolyzer using graphite felt, reticulated vitreous carbon and boron-doped diamond as cathodes, J. Electroanal. Chem. 757 (2015) 225-229.

[24] P. Ma, H. Ma, A. Galia, S. Sabatino, O. Scialdone, Reduction of oxygen to H_2O_2 at carbon felt cathode in undivided cells. Effect of the ratio between the anode and the cathode surfaces and of other operative parameters, Sep. Purif. Technol. 208 (2019) 116-122.

[25] C.A. Martínez-Huitle, M. Rodrigo, I. Sirés, O. Scialdone, Single and coupled electrochemical processes and reactors for the abatement of organic water pollutants: A critical review, Chem. Rev. 115 (2015) 13362-13407.

[26] D. Clematis, M. Panizza, Electrochemical oxidation of organic pollutants in low conductive solutions, Curr. Opinion Electrochem. 26 (2021) 100665.

[27] G.R.P. Malpass, A.J. Motheo, Recent advances on the use of active anodes in environmental electrochemistry, Curr. Opinion Electrochem. 27 (2021) 100689.

[28] S.C. Perry, D. Pangotra, L. Vieira, L.I. Csepei, V. Sieber, L. Wang, C. Ponce de León, F.C. Walsh, Electrochemical synthesis of hydrogen peroxide from water and oxygen, Nat. Rev. Chem. 3 (2019) 442-458.

[29] O. González-Pérez, J.M. Bisang, Electrochemical synthesis of hydrogen peroxide with a three-dimensional rotating cylinder electrode, J. Chem. Technol. Biotechnol. 89 (2014) 528-535.

[30] O. González-Pérez, J.M. Bisang, Alkaline peroxide electrosynthesis by oxygen reduction using an acid anolyte in a divided reactor with a three-dimensional rotating cylinder cathode and two-phase flow induced by centrifugal force, J. Chem. Technol. Biotechnol. 91 (2016) 165-170.

[31] J.L. Arredondo, F.F. Rivera, J.L. Nava, Silver recovery from an effluent generated by plating industry using a rotating cylinder electrode (RCE), Elecrochim. Acta 147 (2014) 337-342.

[32] A. Recéndiz, S. León, J.L. Nava, F.F. Rivera, Mass transport studies at rotating cylinder electrode during zinc removal from dilute solutions, Electrochim. Acta 56 (2011) 1455-1459.

[33] F.F. Rivera, J.L. Nava, M.T. Oropeza, A. Recéndiz, G. Carreño, Mass transport studies at rotating cylinder electrode: Influence of the inter-electrode gap, Electrochim. Acta 55 (2010) 3275-3278.

[34] M. Rosales, J.L. Nava, Simulations of Turbulent Flow, Mass transport, and tertiary current distribution on the cathode of a rotating cylinder electrode reactor in continuous operation mode during silver deposition, J. Electrochem. Soc. 164 (2017) E3345-E3353.

[35] M. Rosales, T. Pérez, J.L. Nava, Computational fluid dynamic simulations of turbulent flow in a rotating cylinder electrode reactor in continuous mode of operation, Electrochim. Acta 194 (2016) 338-345.

[36] D.R. Gabe, F.C. Walsh, The rotating cylinder electrode: a review of development, J. Appl. Electrochem. 13 (1983) 3-21.

[37] D.R. Gabe, G.D. Wilcox, J. González-García, F.C. Walsh, The rotating cylinder electrode: its continued development and application, J. Appl. Electrochem. 28 (1998) 759-780.

[38] Z.G. Aguilar, O. Coreño, M. Salazar, I. Sirés, E. Brillas, J.L. Nava, Ti|Ir–Sn–Sb oxide anode: Service life and role of the acid sites content during water oxidation to hydroxyl radicals, J. Electroanal. Chem. 820 (2018) 82-88.

[39] G. Eisenberg, Colorimetric determination of hydrogen peroxide, Ind. Eng. Chem. Anal. Ed. 15 (1943) 327-328.

[40] F.C. Walsh, Determination of the normalised space velocity for continuous stirred tank electrochemical reactors. Electrochim. Acta 38 (1993) 465-468.

Table 1

Mass transport characterization ($k_m a = bU^c$) during the ORR from dissolved O_2 to yield H_2O_2. A 0.5 M Na_2SO_4 solution at pH 3 and 298 ± 2 K, saturated with 0.25 mM O_2, was used.

	C_{cloth} RCE	BDD plate[a]	GF[a]	RVC[a]
Open to the atmosphere	$0.0042U^{0.22}$	$0.0007U^{0.84}$	$0.0012U^{1.56}$	$0.011U^{0.93}$
N_2 overlying atmosphere	$0.0028U^{0.31}$			

[a] Evaluated through DPV technique in the filter-press type cell (FM01-LC) with a polymeric turbulence promoter between the electrodes [23].

Figure captions

Fig. 1. Isometric and (b) upper view of the RCE reactor, and (c) experimental setup.

Fig. 2. Cathodic polarization curves obtained in the RCE reactor operated in batch mode through the DPV technique. (a) Reactor open to the atmospheric air, and (b) use of an N_2 overlying atmosphere (closed reactor). A 0.5 M Na_2SO_4 at pH 3 and 298 ± 2 K, saturated with 0.25 mM O_2 by sparging air for a long time before each analysis, was employed. The scan rate was fixed at 5 mV s^{-1}, with a pulse height of 1.0 mV and a pulse width of 5.0 ms.

Fig. 3. Logarithmic $k_m a$ vs. U plot to characterize the mass transport for the dissolved O_2 reduction obtained from the analysis of curves in Fig. 2, in the presence (curve *a*) and absence (*b*) of overlying air.

Fig. 4. Influence of the peripheral velocity on the accumulated dissolved O_2 concentration reached at t = 15 min using an open RCE reactor at E_{cath} = -0.46 V vs. SHE with no air pumping. A 0.05 M Na_2SO_4 solution at pH 3 and 298 ± 2 K was employed.

Fig. 5. Influence of peripheral velocity on the (a) accumulated H_2O_2 concentration, (b) current efficiency, and (c) electrolytic energy consumption using the same RCE reactor and conditions described in Fig. 4.

Fig. 6. Same trials described in Fig. 5 but using a closed RCE reactor (i.e., N_2 overlying atmosphere).

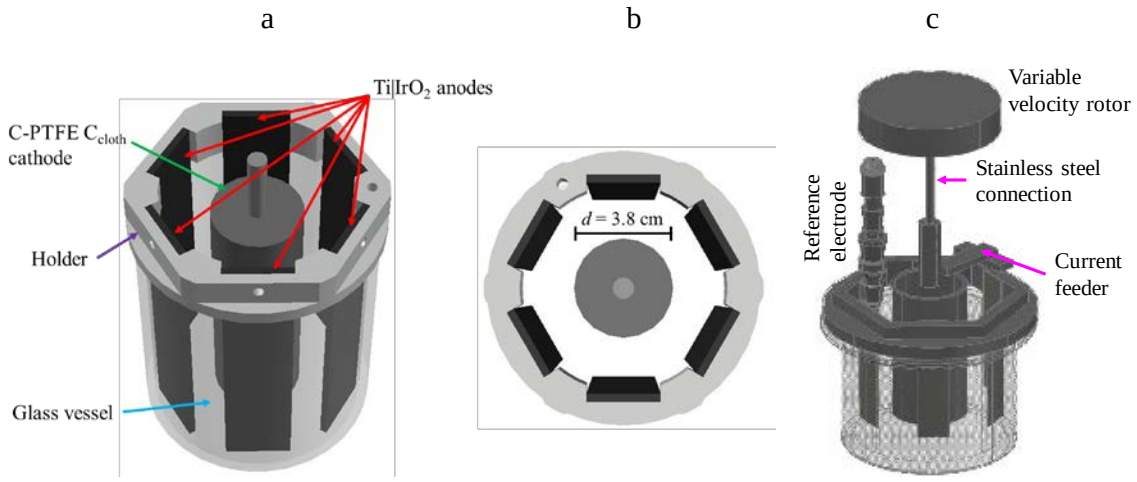
a
b
c
Ti|IrO2 anodes
C-PTFE Ccloth cathode
Holder
Glass vessel
d = 3.8 cm
Variable velocity rotor
Stainless steel connection
Reference electrode
Current feeder

Fig 1

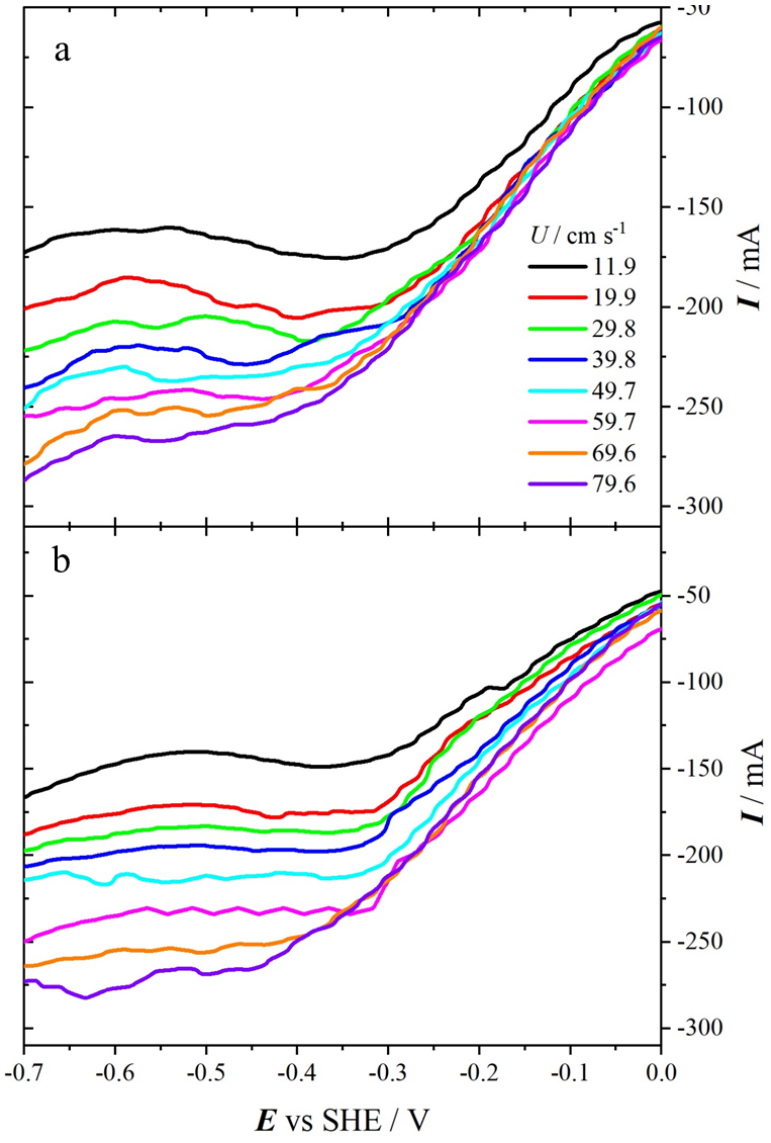
a
b
U / cm s-1
11.9
19.9
29.8
39.8
49.7
59.7
69.6
79.6
I / mA
E vs SHE / V
-0.7
-0.6
-0.5
-0.4
-0.3
-0.2
-0.1
0.0
-50
-100
-150
-200
-250
-300

Fig. 2

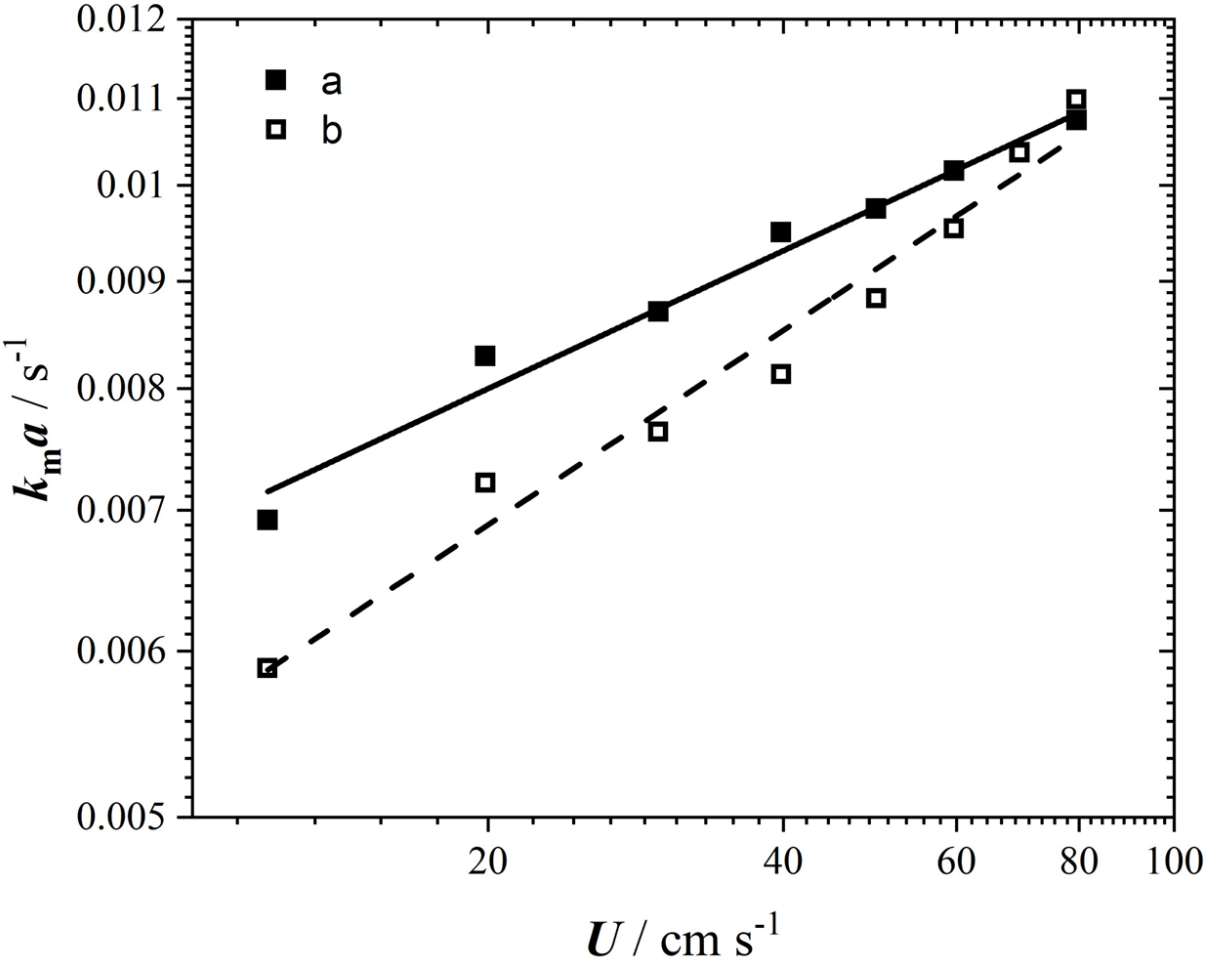
0.012
0.011
0.01
0.009
0.008
0.007
0.006
0.005
a
b
$k_m a$ / s^{-1}
20
40
60
80
100
U / cm s^{-1}

Fig. 3

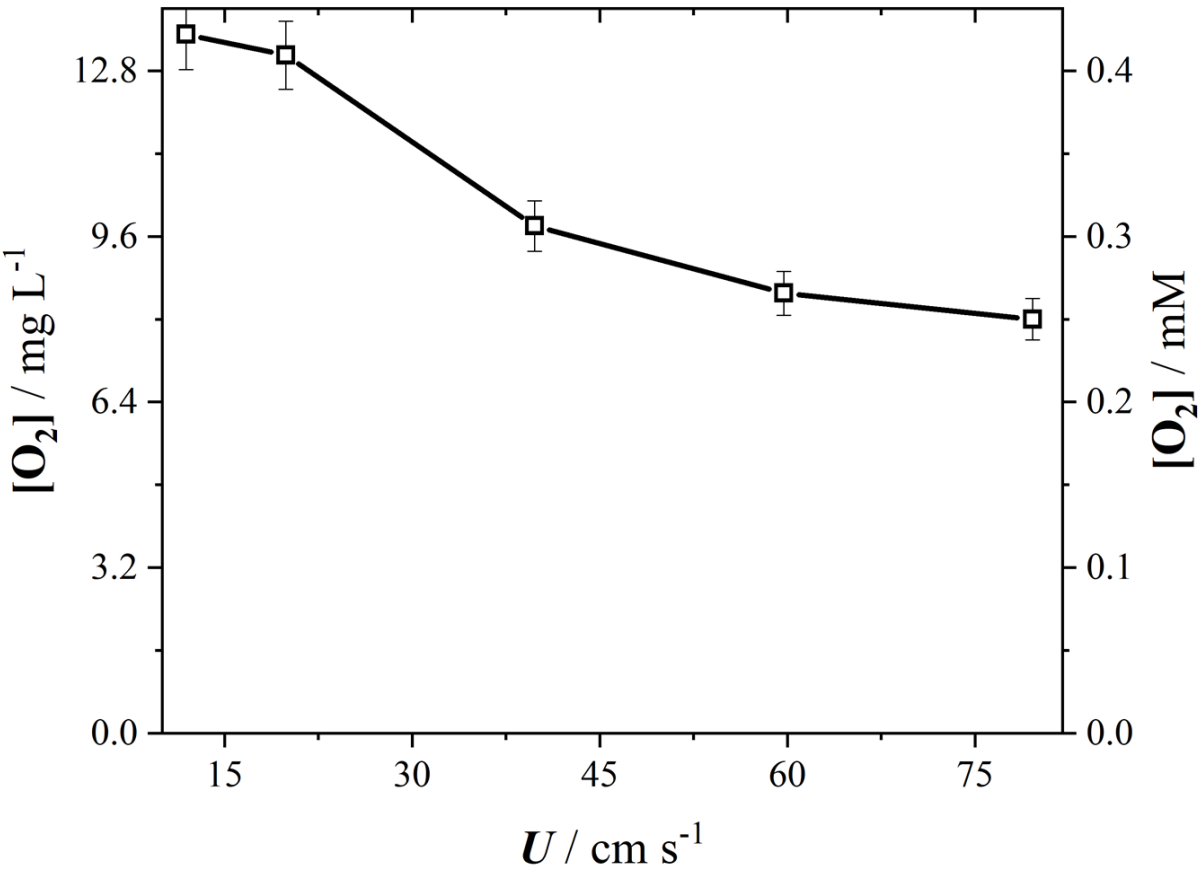

Fig. 4

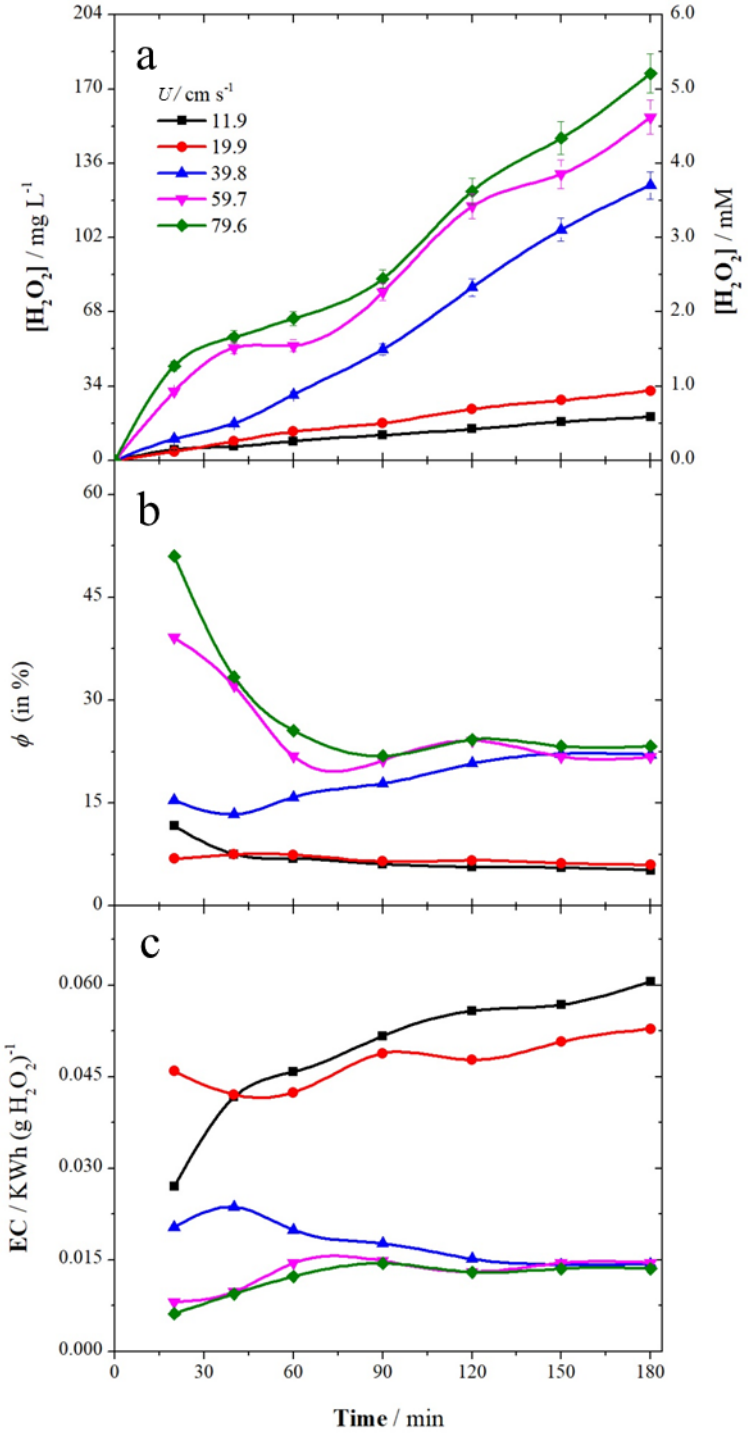
a
b
c
U / cm s-1
11.9
19.9
39.8
59.7
79.6
[H2O2] / mg L-1
[H2O2] / mM
ϕ (in %)
EC / KWh (g H2O2)-1
Time / min
0
34
68
102
136
170
204
0.0
1.0
2.0
3.0
4.0
5.0
6.0
15
30
45
60
0.000
0.015
0.030
0.045
0.060
0
30
60
90
120
150
180

Fig. 5

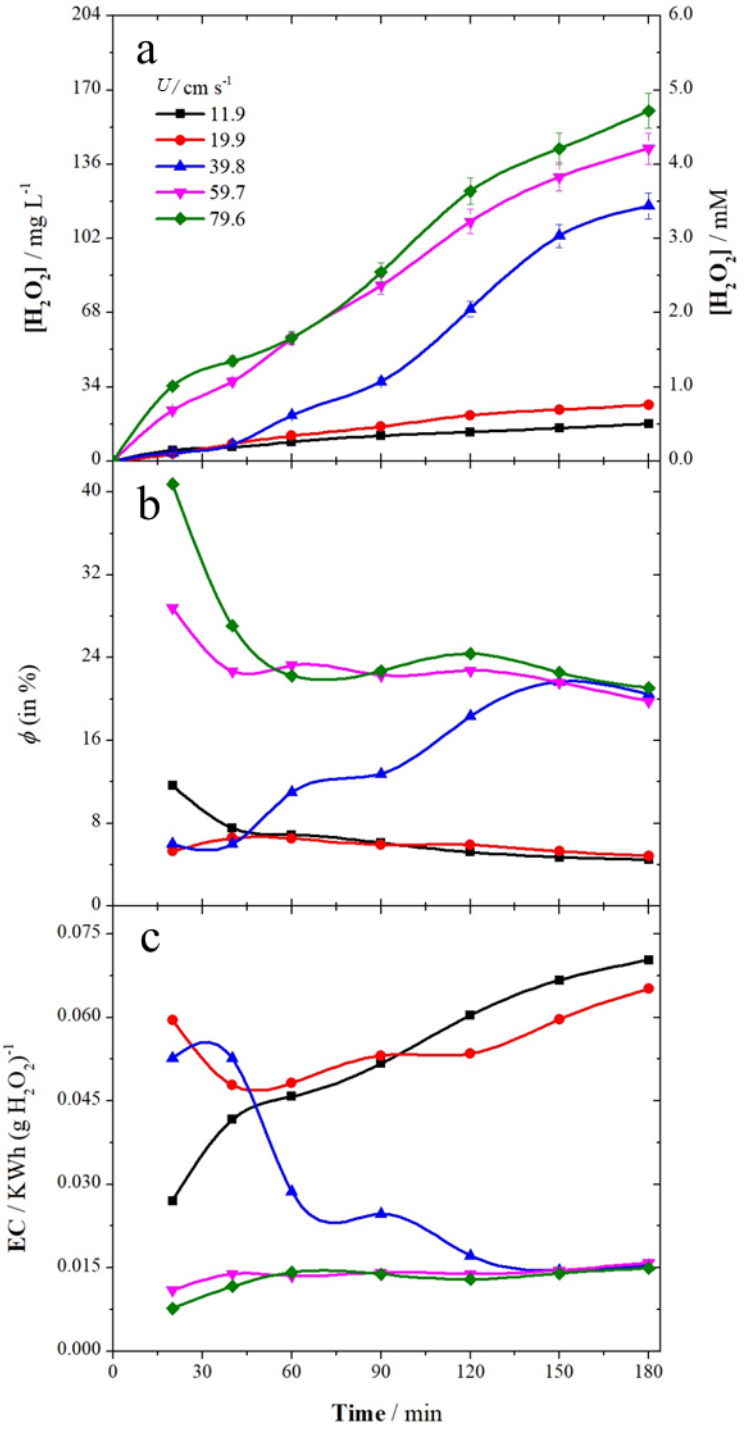
a
b
c
U / cm s-1
11.9
19.9
39.8
59.7
79.6
[H2O2] / mg L-1
[H2O2] / mM
ϕ (in %)
EC / KWh (g H2O2)-1
Time / min
204
170
136
102
68
34
0
6.0
5.0
4.0
3.0
2.0
1.0
0.0
40
32
24
16
8
0
0.075
0.060
0.045
0.030
0.015
0.000
0
30
60
90
120
150
180

Fig. 6